Maximum entropy and population heterogeneity in continuous cell cultures meet experimental data, preliminary results

September 26, 2019

1 Materials and Method

1.1 Model framework

The model framework used is detaily explained in (Fernandez-de Cossio-Diaz et al., 2017) and (Fernandez-de Cossio-Diaz & Mulet, 2019).

1.2 Experimental data

Experimental data were taken from (Rath, 2017). In this work, the author performed 6 continuous cultures, (A, B, C, D, E, F), with the cell line AGE1.HN.AA1. The parental line AGE1.HN was established by the company ProBioGen (ProBioGen AG, Berlin, Germany) from a tissue sample of a human brain. All culture's feed mediums were based on the standard 42-Max-UB-medium, which is serum-free and was specially developed for the AGE1.HN cell line $Table$ 1. The experiments were run under various conditions, differing mainly in the dilution rate (D) and the feed medium composition of glucose (GLC), glutamine (GLN) and galactose ($GAL/GALC$) $Table$ 2.

For each experiment, a steady-state condition was reached, (A, B, C, D, E, $F01$), and several observables was reported $Tables\ 3-4$. Particularly relevant for this work was the growth rate (μ), D, the viable cell density (Xv) and the medium concentration (s) and derived uptake rate (u/q) for a set of metabolites (GLC, lactose (LAC), GLN, ammonium ($NH4$), GAL, pyruvate (PYR), glutamate (GLU), alanine (ALA), asparagine (ASP)). A unit conversion was required to make experimental data and our model compatible. For this propose the only external data needed was the cell mass density. It was used 0.25 pgDW/ μm^3 (Niklas et al., 2011).

1.3 Preparing GEMs

In order to preliminary evaluate the capacity of the model to reproduce the experimental data, two Genome-scale Metabolic Models (GEM) were prepared.

1.3.1 Recon3D

Recon3D represents the most comprehensive human metabolic network model to date (Brunk et al., 2018). The model, Recon3DModel_301.mat, was downloaded from http://vmh.life. The original biomass equation was modified to adjust the biomass demand reported by (Niklas et al., 2013) for the parental line AGE1_HN. All the other original demands from *Recon3D* were deactivated. An extra reaction representing the maintenance demand, not associated with growth, of atp was set according to (Fernandez-de Cossio-Diaz & Mulet, 2019). All the fluxes representing exchangeable metabolites (external reactions) were set as reversible (lb and ub set to a large number), so the only effective bound constraints are the ones produced by the chemostat consideration (Fernandez-de Cossio-Diaz & Mulet, 2019). Additionally, to include the molecular crowding constraints, we map (Shlomi et al., 2011) enzymatic costs, initially defined for *Recon1*, to *Recon3D*.

Pursuing to reproduce the conditions of the different steady states, the external concentrations of the exchangeable metabolites were set using the data from *Tables* $1-2$. Additionally, external concentrations of salts, oxygen, and other metabolites not specified in the medium were set to a large number. Particularly, *Recon3D* was unable to grow without pe_hs[e], phosphatidylethanolamine, (or similar) lipid in the feed medium. Later we will discuss the impact of this metabolite in the medium.

1.3.2 CHO

Chinese hamster ovary (*CHO*) host cell-lines GEM was obtained from (Hefzi et al., 2016) and was set up in (Fernandez-de Cossio-Diaz & Mulet, 2019). The external metabolite concentrations were set to the values indicated in *Table* $1-2$, similar to Recon3D. Also, a few extra metabolites, taken from (Fernandez-de Cossio-Diaz & Mulet, 2019) were included in the feed medium. An important difference from Recon3D was that *CHO* is able to grow without pe_hs[e], named in *CHO* as pe_cho_e.

2 Results

2.1 Low concentrations of phosphatidylethanolamine

Because phosphatidylethanolamine isn't a reported component of the 42-Max-UB-medium, *Tabla* 1, and it can be a carbon source for the $GEMs$, its concentration was set first to the lowest value possible. For $Recon3D$ it was fixed to 0.5mM (a handpicked value) and for CHO it wasn't present in the feed medium at all.

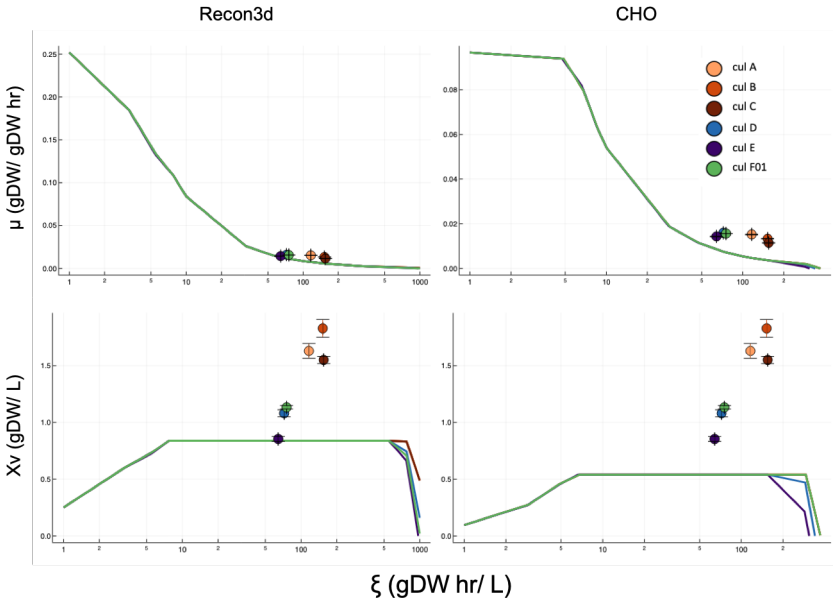

Figure 1: FBA results showing the growth rate, μ, and the viable cell density, Xv, dependence of ξ for the six steady states. The solid lines represent the model predictions and the colored points show the experimental results. The model data was obtained for feed mediums with 0.5mM ($Recon3D$) and 0.0mM (CHO) concentration of phosphatidylethanolamine

Flux balance analysis with molecular crowding (FBA) was performed similarly to (Fernandez-de Cossio-Diaz & Mulet, 2019). Plots of μ and Xv as a function of ξ are shown in $Figure$ 1. Both networks failed to reach the experimental values for both observables. In the case of Xv, in all the explored ξ range (from 1 to 1000 gDW hr/ L) the value was underestimated. This result may have several causes. One could be that the GEM has a "too expensive" biomass equation. We mean that one or more biomass required precursors might be overestimated. However, this reason seems hard to sustain because we modified the $Recon3D$ biomass equation with the reported anabolic biomass demand for AGE1.HN.AA1 (Niklas et al., 2013). We used the reported anabolic

demand of proteins, lipids, DNA, RNA, and carbohydrates to fix the total demand of these same groups in the original *Recon3D* biomass equation. For *CHO* we kept the biomass equation unmodified. Nonetheless, a modification in the biomass equation would be an elegant way to solve the problem. Another plausible cause could be a big difference between the model's frameworks. But, both works model the chemostat in an equivalent fashion, as can be seen when comparing equations 1 with 3.25, and 2 with 3.28 and 3.29, from (Fernandez-de Cossio-Diaz et al., 2017) and (Rath, 2017) respectively.

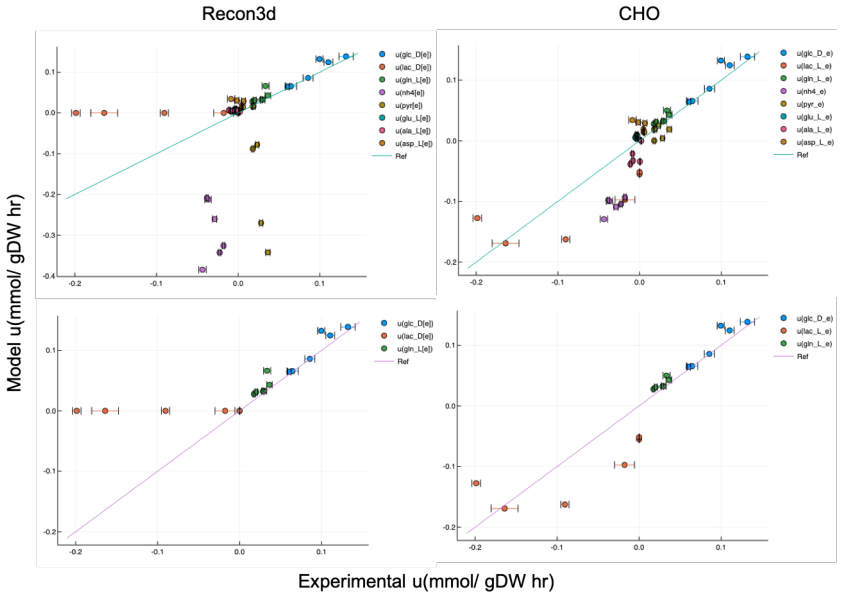

Figure 2: Correlations of all the experimental uptakes, upper graphs, and a selected subset, inferior graphs, respect to the predicted value from *FBA* with 0.5mM (*Recon3D*) and 0.0mM (*CHO*) concentration of phosphatidylethanolamine.

Moreover, other parameter than can affect Xv is the bleeding coefficient, ϕ, defined in perfusion systems as the fraction of cells that escape from the culture through a cell-retention device (Fernandez-de Cossio-Diaz et al., 2017). Because, (Rath, 2017) doesn't report the use of any retention devise in the cultures this parameter was taken as 1.0, but lower values will cause to increment the predicted value of Xv by the model. Finally, it needs to be taken into consideration that we are using *GEMs* that are not directed curated for the working cell line. In fact, a crucial phenotypic feature reported for AGE1.HN.AA1 like the impossibility of growth in *GLN* free mediums (Rath, 2017) is not reproduced by the used *GEMs*. This is, by far, the most difficult factor to solve, because the curation of a genome-scale metabolic network is a very laborious process.

On the other hand, correlations of experimental and modeled uptakes, *Figure* 2,

were performed. The graphs show better results for the uptakes of GLC and GLN, and worse correlations for uptakes such as PYR, $NH4$ and LAC for both $GEMs$. In general, CHO had better correlations than $Recon3D$. This could be, maybe, explained because $Recon3D$ is a general GEM, allowing the model to access to all the human genome repertory, a fact that is not accurate for a cell in the *in vivo* scenario. Additionally, CHO was curated for a defined cell line, representing a more restricted and realistic network. Anyway, it is remarkable that the models reproduce uptakes like GLC and GLN regarding all the previous consideration.

2.2 High concentrations of phosphatidylethanolamine

To avoid the undesired Xv and μ underestimation, a less realistic scenario was considered. An extra carbon source was put in excess in the feed medium. We select the phosphatidylethanolamine (PE) because it was already introduced in the $Recon3D$ medium, do to the incapacity of this GEM to growth without this (or similar) metabolite, and it is an usable carbon source. So, the feed medium concentration of PE was set to a high value, 20 mM (a handpicked value), for both GEMs.

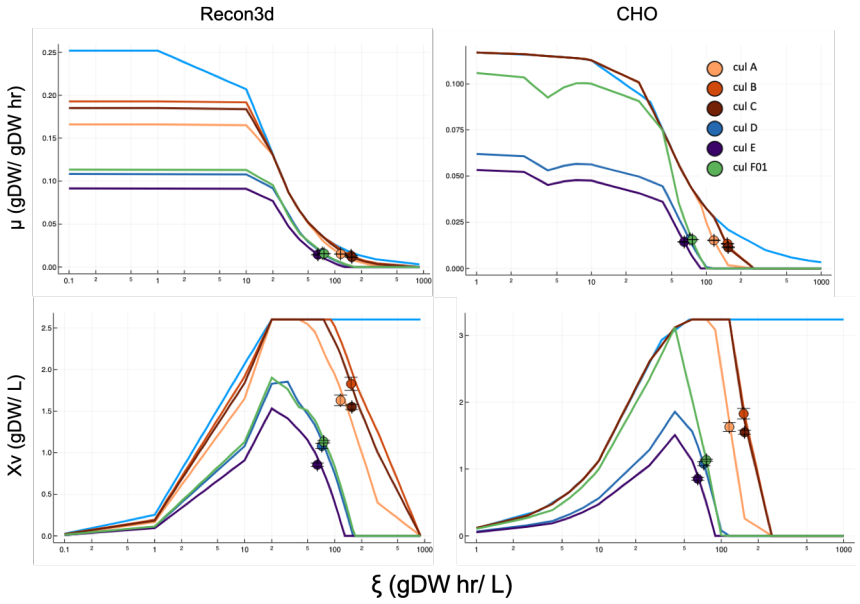

Figure 3: EP and FBA results showing the growth rate, μ, and the viable cell density, Xv, dependence of ξ for the six culture conditions. The solid lines represent the model predictions and the color points show the experimental results. FBA results are shown as the solid light blue line. EP β parameters was chosen, for each culture, so that the experimental μ coincides with the modeled one

This time, additionally to FBA, the expected propagation (EP) algorithm was used to introduce a population heterogeneity factor (Fernandez-de Cossio-Diaz & Mulet, 2019). $Figure$ 3 shows the results of both methods for $Recon3D$ and CHO. As can be appreciated, FBA (lite blue solid line) overestimate the experimental results. This is consistent with the fact that we put a carbon source, PE, in a high concentration, allowing the network to reach higher μ and Xv values.

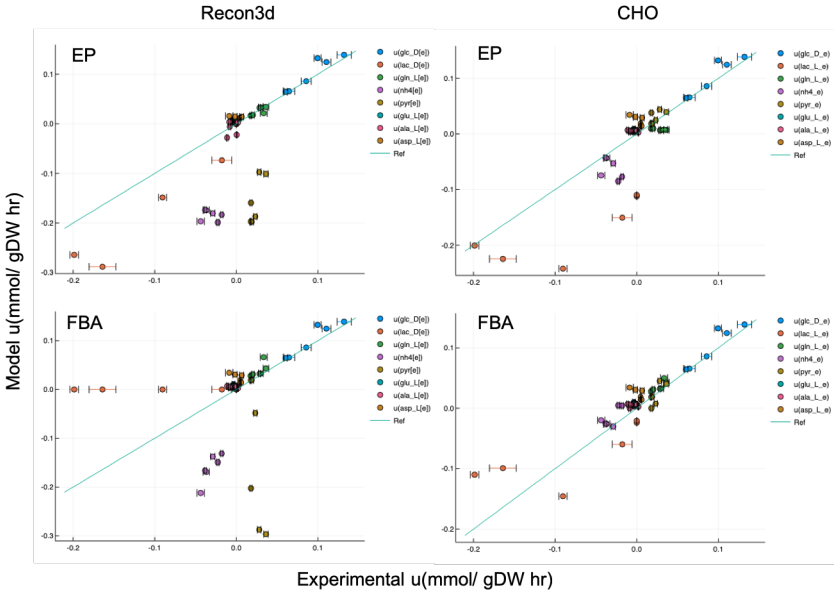

Figure 4: Correlations of all the experimental uptakes compared with the predicted value from EP and FBA for $GEMs$ with 20mM concentration of phosphatidylethanolamine.

On the other hand, EP can be tuned through parameter β. This parameter can be interpreted as a measurement of the cell heterogeneity in the culture (Fernandez-de Cossio-Diaz & Mulet, 2019). β values closer to zero indicate higher heterogeneity in the culture, or that the cells can explore more uniformly the space of possibles metabolic states. By contrast, larger β values will be approaching the EP model result to FBA result, meaning that no cell heterogeneity is accounted at all. As is appreciated in $Figure$ 3, considering different β values allow the EP model to reproduce the measured μ and Xv. This is an interesting result for several reasons. First, it improves the FBA solution. FBA is insensible to the different experimental conditions, as shown in $Figure$ 1 and 3. This means that it does not vary the observable predictions, mainly Xv, after changing the particular culture conditions, metabolite feed medium concentrations and dilution rate. This occurs for both situations, low and high concentration of PE, at least with this GEMs and settings. This

could, maybe, be explained because FBA, as used in this work, returns an optimal metabolic state that maximizes μ. However, it is possible that many different states maximize μ, a not unique solution scenario, and this can make the network robust enough to be insensible to the changes in the input.

Because EP introduces the heterogeneity factor, a better exploration of the space of feasible metabolic states is now possible. There are many factors that can influence the heterogeneity of a population of cells (Elowitz et al., 2002; Tzur et al., 2009; Huh & Paulsson, 2011; Delvigne et al., 2014; King et al., 2016; Wang et al., 2016; González-Cabaleiro et al., 2017; Fernandez-de Cossio-Diaz et al., 2019). The experimental results can be then interpreted, not only because different input conditions lead to an unique different metabolic state, but because these same changes in the input modified the likelihood distribution of the feasible metabolic states through the cell population. This interpretation is qualitatively different from what FBA represents.

Furthermore, the correlation of experimental and modeled uptakes was performed, $Figure$ 4, for both methods. Again, the best correlations were achieved for the uptakes of GLC and GLN. A small improvement in the general results can be observed for EP compared with FBA, in particular for $Recon3D$. The causes that are driven these results could be the same disused in the previous section.

3 References

Brunk, E., Sahoo, S., Zielinski, D. C., Altunkaya, A., Dräger, A., Mih, N., ... Palsson, B. O. (2018). Recon3D enables a three-dimensional view of gene variation in human metabolism. *Nature Biotechnology*, *36*(3), 272–281. Retrieved from `http://dx.doi.org/10.1038/nbt.4072` doi: 10.1038/nbt.4072

Delvigne, F., Zune, Q., Lara, A. R., Al-Soud, W., & Sørensen, S. J. (2014). Metabolic variability in bioprocessing: Implications of microbial phenotypic heterogeneity. *Trends in Biotechnology*, *32*(12), 608–616. Retrieved from `http://dx.doi.org/10.1016/j.tibtech.2014.10.002` doi: 10.1016/j.tibtech.2014.10.002

Elowitz, M. B., Levine, A. J., Siggia, E. D., & Swain, P. S. (2002). Stochastic gene expression in a single cell. *Science*, *297*(5584), 1183–1186. doi: 10.1126/science.1070919

Fernandez-de Cossio-Diaz, J., Leon, K., & Mulet, R. (2017). Characterizing steady states of genome-scale metabolic networks in continuous cell cultures. *PLoS Computational Biology*, *13*(11), 1–22. doi: 10.1371/journal.pcbi.1005835

Fernandez-de Cossio-Diaz, J., & Mulet, R. (2019). Maximum entropy and population heterogeneity in continuous cell cultures. *PLoS Computational Biology*, *15*(2), 1–22. Retrieved from `http://arxiv.org/abs/1807.03982` doi: 10.1371/journal.pcbi.1006823

Fernandez-de Cossio-Diaz, J., Mulet, R., & Vazquez, A. (2019). Cell population heterogeneity driven by stochastic partition and growth optimality. *Scientific Reports*, *9*(1), 1–17. doi: 10.1038/s41598-019-45882-w

González-Cabaleiro, R., Mitchell, A. M., Smith, W., Wipat, A., & Ofiteru, I. D. (2017). Heterogeneity in pure microbial systems: Experimental measurements and modeling. *Frontiers in Microbiology*, *8*(SEP), 1–8. doi: 10.3389/fmicb.2017.01813

Hefzi, H., Ang, K. S., Hanscho, M., Bordbar, A., Ruckerbauer, D., Lakshmanan, M., ... Lewis, N. E. (2016). A Consensus Genome-scale Reconstruction of Chinese Hamster Ovary Cell Metabolism. *Cell Systems*, *3*(5), 434–443.e8. doi: 10.1016/j.cels.2016.10.020

Huh, D., & Paulsson, J. (2011). Random partitioning of molecules at cell division. *Proceedings of the National Academy of Sciences of the United States of America*, *108*(36), 15004–15009. doi: 10.1073/pnas.1013171108

King, Z. A., Lu, J., Dräger, A., Miller, P., Federowicz, S., Lerman, J. A., ... Lewis, N. E. (2016). BiGG Models: A platform for integrating, standardizing and sharing genome-scale models. *Nucleic Acids Research*, *44*(D1), D515–D522. doi: 10.1093/nar/gkv1049

Niklas, J., Priesnitz, C., Rose, T., Sandig, V., & Heinzle, E. (2013). Metabolism and metabolic burden by a 1 -antitrypsin production. *Metabolic Engineering*, *16*, 103–114. Retrieved from http://dx.doi.org/10.1016/j.ymben.2013.01.002 doi: 10.1016/j.ymben.2013.01.002

Niklas, J., Schräder, E., Sandig, V., Noll, T., & Heinzle, E. (2011). Quantitative characterization of metabolism and metabolic shifts during growth of the new human cell line AGE1.HN using time resolved metabolic flux analysis. *Bioprocess and Biosystems Engineering*, *34*(5), 533–545. doi: 10.1007/s00449-010-0502-y

Rath, A. (2017). *Characterisation of cell growth, metabolism and recombinant protein production during transient and steady state conditions for the human cell line AGE1.HN-AAT* (Doctoral dissertation). Retrieved from https://pure.mpg.de/pubman/item/item_2508673_4

Shlomi, T., Benyamini, T., Gottlieb, E., Sharan, R., & Ruppin, E. (2011). Genome-scale metabolic modeling elucidates the role of proliferative adaptation in causing the Warburg effect. *PLoS computational biology*, *7*(3), e1002018. Retrieved from http://www.ncbi.nlm.nih.gov/pubmed/21423717%0Ahttp://www.pubmedcentral.nih.gov/articlerende doi: 10.1371/journal.pcbi.1002018

Tzur, A., Kafri, R., LeBleu, V. S., Lahav, G., & Kirschner, M. W. (2009). Cell growth and size homeostasis in proliferating animal cells. *Science*, *325*(5937), 167–171. doi: 10.1126/science.1174294

Wang, J., Cazzato, E., Ladewig, E., Frattini, V., Rosenbloom, D. I., Zairis, S., ... Rabadan, R. (2016). Clonal evolution of glioblastoma under therapy. *Nature Genetics*, *48*(7), 768–776. doi: 10.1038/ng.3590

4 Appendix

Substance	Value	Dimension	Analytical method
Pluronic	1.0	g/L	as stated by Xell
NaHCO3	2.1	g/L	as stated by Xell
Osmolality	290.0	$^{mOsm}/_{kg}$	FPDO[a]
pH value	7.4	-	pH meter
GALC	0.5	g/L	AEC[b]
GLC	5.5	g/L	Bioprofile
AMM	0.3	mM	Bioprofile
LAC	0.0	g/L	Bioprofile
PYR	2.9	mM	AEC
GLU	636.9	µM	AEC
ALA	437.1	µM	AEC
ARG	1588.2	µM	AEC
ASN	920.4	µM	AEC
ASP	2197.9	µM	AEC
CYS	963.1	µM	AEC
GLY	1196.0	µM	AEC
HIS	642.7	µM	AEC
ILE	1744.9	µM	AEC
LEU	1893.2	µM	AEC
LYS	1256.0	µM	AEC
MET	601.3	µM	AEC
PHE	1039.4	µM	AEC
PRO	1040.5	µM	AEC
SER	3027.4	µM	AEC
THR	1502.4	µM	AEC
TRP	383.8	µM	AEC
TYR	1109.7	µM	AEC
VAL	1811.9	µM	AEC

a: freezing point depression osmometer (FPDO); b: anion exchanger chromatography (AEC);

Table 1: Measured composition of the 42-MAX-UB standard medium. Extracted from (Rath, 2017)

Exp. ID	*DR* ($^{1}/_{h}$)	Preculture (passage no.)	GLC (mM)	GLN (mM)	GALC (mM)
A	0.0140	7	10	5	3
B	0.0120	7	10	5	3
C	0.0100	5	10	5	3
D	0.0150	8	10	2	3
E	0.0133	4	8	2	3
F01	0.0150	10	10	5	0

Table 2: The dilution rates, preculture ages and the 42-Max-UB-medium modified components concentrations used in (Rath, 2017) for the 6 steady states. Table adapted from (Rath, 2017)

Variable	Exp. A		Exp. B		Exp. C		Exp. D		Exp. E	
	Average ± SD	Rel. SD (%)	Average ± SD	Rel. SD (%)	Average ± SD	Rel. SD (%)	Average ± SD	Rel. SD (%)	Average ± SD	Rel. SD (%)
Setpoints:										
DR (1/h)	0.0140	-	0.0120	-	0.0100	-	0.0150	-	0.0133	-
GLC feed conc. (mM)	10.0	-	10.0	-	10.0	-	10.0	-	8.0	-
GLN feed conc. (mM)	5.0	-	5.0	-	5.0	-	2.0	-	2.0	-
GALC feed conc. (mM)	3.0	-	3.0	-	3.0	-	3.0	-	3.0	-
GLC/GLN ratio (mol/mol)	2	-	2	-	2	-	5	-	4	-
X_V (E6 cells/mL)	2.490 ± 0.100	4.0	2.745 ± 0.118	4.3	2.735 ± 0.056	2.0	1.489 ± 0.043	2.9	0.998 ± 0.025	2.5
X_D (E6 cells/mL)	0.210 ± 0.032	15.2	0.291 ± 0.021	7.4	0.378 ± 0.047	12.5	0.086 ± 0.006	6.5	0.075 ± 0.014	18.5
CV_v (μL/mL)	6.56 ± 0.48	7.4	7.19 ± 0.67	9.4	6.23 ± 0.21	3.4	4.33 ± 0.27	6.3	3.40 ± 0.17	4.9
μ (1/h)	0.0152 ± 0.0002	1.2	0.0133 ± 0.0001	1.1	0.0114 ± 0.0002	1.4	0.0159 ± 0.0001	0.6	0.0143 ± 0.0002	1.4
CD (μm)	17.1 ± 0.25	1.5	17.2 ± 0.19	1.1	16.3 ± 0.24	1.5	17.7 ± 0.30	1.5	18.7 ± 0.20	1.1
GLC (mM)	0.0 ± 0.00	-	0.0 ± 0.00	-	0.0 ± 0.00	-	0.0 ± 0.00	-	0.0 ± 0.00	-
LAC (mM)	2.1 ± 1.52	-	0.0 ± 0.00	-	0.0 ± 0.00	-	12.5 ± 0.60	5.0	12.7 ± 0.40	3.0
GLN (mM)	0.8 ± 0.08	10.0	0.5 ± 0.02	3.5	0.6 ± 0.04	7.3	0.5 ± 0.10	11.1	0.5 ± 0.10	13.7
AMM (mM)	3.4 ± 0.22	6.7	5.5 ± 0.19	3.5	5.9 ± 0.09	1.5	1.5 ± 0.03	2.1	1.6 ± 0.02	1.6
GALC (mM)	1.9 ± 0.08	4.5	1.9 ± 0.06	2.9	1.7 ± 0.02	0.9	2.1 ± 0.10	2.5	2.4 ± 0.10	3.2
PYR (mM)	0.2 ± 0.00	1.8	0.1 ± 0.00	3.2	0.1 ± 0.00	3.2	0.3 ± 0.04	12.6	1.1 ± 0.10	5.3
GLU (mM)	1.2 ± 0.08	6.2	1.3 ± 0.01	0.5	1.0 ± 0.05	5.0	0.7 ± 0.10	12.9	0.8 ± 0.10	12.8
ALA (mM)	1.4 ± 0.09	6.4	0.2 ± 0.03	13.8	0.1 ± 0.01	14.2	0.3 ± 0.02	8.9	1.0 ± 0.05	5.2
ASP (mM)	1.6 ± 0.06	3.9	1.5 ± 0.05	3.2	1.3 ± 0.02	1.2	2.4 ± 0.17	7.1	2.8 ± 0.30	10.8
A1AT (mg/L)	57.9 ± 3.03	5.2	81.0 ± 9.21	11.4	72.1 ± 1.09	1.5	50.9 ± 1.50	2.9	44.6 ± 2.80	6.2
$Y_{CVv/glc}$ (μL/mmol)	711 ± 47	6.6	827 ± 77	9.4	753 ± 17	2.3	482 ± 30	6.3	518 ± 18	3.5
$Y_{CVv/gln}$ (μL/mmol)	1679 ± 140	8.3	1770 ± 145	8.2	1601 ± 52	3.3	3617 ± 215	6.0	2837 ± 201	7.1
$Y_{lac/glc}$ (mol/mol)	0.2 ± 0.15	-	0.0 ± 0.01	-	0.0 ± 0.00	-	1.2 ± 0.10	5.3	1.8 ± 0.10	3.2
$Y_{amm/gln}$ (mol/mol)	0.8 ± 0.05	6.6	1.2 ± 0.04	3.6	1.3 ± 0.03	1.9	1.0 ± 0.05	4.9	1.1 ± 0.10	4.8
$Y_{ala/gln}$ (mol/mol)	0.2 ± 0.02	9.5	0.0 ± 0.00	-	0.0 ± 0.00	-	0.0 ± 0.00	-	0.6 ± 0.04	7.9
q_{GLC} (nmol/μL h)[a]	21.43 ± 1.56	7.3	16.17 ± 1.76	10.9	15.13 ± 0.51	3.4	33.05 ± 2.17	6.6	27.64 ± 1.33	4.8
q_{LAC} (nmol/μL h)[a]	-4.43 ± 3.05	-	0.00 ± 0.00	-	0.00 ± 0.00	-	-41.23 ± 4.13	10.0	-49.68 ± 1.30	2.6
q_{GLN} (nmol/μL h)[a]	9.10 ± 0.82	9.0	7.55 ± 0.72	9.5	7.12 ± 0.31	4.3	4.40 ± 0.28	6.4	5.07 ± 0.41	8.1
q_{AMM} (nmol/μL h)[a]	-7.19 ± 0.67	9.3	-9.21 ± 0.97	10.5	-9.55 ± 0.30	3.2	-4.48 ± 0.35	7.8	-5.66 ± 0.33	5.9
q_{GALAC} (nmol/μL h)[a]	1.94 ± 0.21	10.8	1.55 ± 0.22	14.3	2.46 ± 1.26	51.1	1.92 ± 0.24	12.3	1.61 ± 0.37	23.3
q_{PYR} (nmol/μL h)[a]	5.82 ± 0.52	8.9	4.70 ± 0.57	12.1	4.48 ± 0.11	2.4	9.10 ± 0.64	7.1	7.04 ± 0.55	7.8
q_{GLU} (nmol/μL h)[a]	-1.31 ± 0.18	14.0	-1.05 ± 0.10	9.4	-0.52 ± 0.09	17.9	-0.71 ± 0.31	43.5	-0.88 ± 0.38	43.8
q_{ALA} (nmol/μL h)[a]	-2.14 ± 0.27	12.8	0.39 ± 0.03	6.7	0.54 ± 0.03	5.9	0.10 ± 0.12	127.8	-2.81 ± 0.26	9.4
q_{ASP} (nmol/μL h)[a]	1.19 ± 0.19	15.9	1.20 ± 0.10	8.1	1.49 ± 0.05	3.5	-0.41 ± 0.62	150.7	-2.16 ± 1.15	53.1
q_{A1AT} (pg/cell d)[a]	-7.87 ± 0.19	2.4	-8.54 ± 1.34	15.7	-6.33 ± 0.19	3.0	-12.31 ± 0.60	4.9	-14.29 ± 1.08	7.5

a: Substrate uptake is indicated by a positive rate, whereas a negative value indicates a production rate.

Table 3: Steady-state values reported by (Rath, 2017) for different parameters from continuous cultivations, varying *GLC* and *GLN* feed concentrations and with 3 mM *GAL*. Table taken from (Rath, 2017)

Variable	Exp. F01	
	Average ± SD	Rel. SD (%)
Setpoints:		
DR (1/h)	0.0150	-
GLC feed conc. (mM)	10	-
GLN feed conc. (mM)	5	-
GALC feed conc. (mM)	0	-
GLC/GLN ratio (mol/mol)	2	-
X_V (E6 cells/mL)	1.701 ± 0.023	1.3
X_D (E6 cells/mL)	0.081 ± 0.004	5.1
CV_v (μL/mL)	4.54 ± 0.24	5.2
μ (1/h)	0.0156 ± 0.0000	0.2
CD (μm)	17.2 ± 0.33	1.9
GLC (mM)	0.0 ± 0.00	-
LAC (mM)	7.8 ± 0.64	8.2
GLN (mM)	1.9 ± 0.18	9.3
AMM (mM)	3.4 ± 0.17	5.1
PYR (mM)	0.4 ± 0.02	6.6
GLU (mM)	1.0 ± 0.05	5.2
ALA (mM)	0.9 ± 0.07	8.2
ASP (mM)	1.9 ± 0.21	10.8
A1AT (mg/L)	44.0 ± 1.71	3.9
$Y_{CVv/glc}$ (μL/mmol)	626 ± 25	4.0
$Y_{CVv/gln}$ (μL/mmol)	1865 ± 201	10.8
$Y_{lac/glc}$ (mol/mol)	0.9 ± 0.07	8.2
$Y_{amm/gln}$ (mol/mol)	1.3 ± 0.04	3.1
$Y_{ala/gln}$ (mol/mol)	0.2 ± 0.02	8.5
q_{GLC} (nmol/μL h)[a]	24.9 ± 1.08	4.3
q_{LAC} (nmol/μL h)[a]	-22.6 ± 1.27	5.6
q_{GLN} (nmol/μL h)[a]	8.4 ± 1.07	12.7
q_{AMM} (nmol/μL h)[a]	-10.9 ± 1.13	10.3
q_{PYR} (nmol/μL h)[a]	4.5 ± 0.31	6.9
q_{GLU} (nmol/μL h)[a]	-0.7 ± 0.15	20.4
q_{ALA} (nmol/μL h)[a]	-1.99 ± 0.33	16.3
q_{ASP} (nmol/μL h)[a]	1.65 ± 0.64	39.0
q_{A1AT} (pg/cell d)[a]	-9.2 ± 0.25	2.7

a: Substrate uptake is indicated by a positive rate, whereas a negative value indicates a production rate.

Table 4: Steady-state values reported by (Rath, 2017) of different parameters from continuous cultivations, varying GLC and GLN feed concentrations and without GAL. Table taken from (Rath, 2017)